International Journal of Latest Research in Science and Technology **ISSN (Online):2278-5299**
Volume 10, Issue 2: Page No.42-52 (2021)
https://www.mnkjournals.com/journal/ijlrst/index.php

ON THE QUESTION OF WAVE MATTER DUALITY

ROGER J. VIEIRA
Private Researcher, Trinidad
vieira.research1@gmail.com

Received: 19August, 2021; Accepted :10 September,2021; Published :19 October, 2021

Abstract: ***Wave matter duality has now moved into the realm of settled science with slit experiments at the core of the debate. The suggestion is that if matter (atoms, molecules) can exhibit wave-like diffraction patterns then surely matter must possess wave properties with the de Broglie equation providing its wavelength. This paper offers a different view of the diffraction patterns observed in slit experiments and demonstrates that wave theory may not be the correct interpretation thus calling into question the very essence of wave matter duality. New concepts and formalisms are introduced all in the context of explaining the physics of slit experiments however these novel methods hold bright promise for further investigation into atomic structures leading to a better understanding of the quantized nature of matter.***

Keywords**-:**Sit experiments, QEM radiation, Field equations, Probability Amplitudes.

I. INTRODUCTION

TO understand why diffraction patterns are observed in slit experiments, one must be aware of the physical phenomena taking place at the diffraction grating. Previously it was assumed that the slits and grating material were passive bystanders in the process of pattern creation and that matter particles exhibiting wave like properties were the source of the interference patterns. It will be shown that the grating material and the slits themselves are the active components in pattern creation and that matter particles simply behave as ordinary massive test particles following the deterministic laws of physics. There is no need to appeal to wave theory to explain these diffraction patterns.

The work is presented in the following order:

II. QEM fields and their origination
III. The field equations
IV. Solutions to the field equations
V. Equations of motion
VI. Particle diffraction
VII. Probability amplitudes
VIII. Gaussian distributions
IX. Experimental verification
X. Conclusions

Sections III and IV present the field equations and their solution utilizing techniques from the literature. Section V presents the equation of motions for massive test particles in QEM fields. Sections VI, VII and VIII present some new methods that are generally applicable to particle diffraction. Probability amplitudes is borrowed from QFT. Six experiments from the literature were studied and results predicted by QEM field theory are compared in section IX Finally interesting conclusions are presented for follow-up.

QEM FIELDS

Energy levels in these experiments are low (65 – 180 mev) which negates high energy scattering and other such phenomena nevertheless it is important to look at a typical energy balance equation.

$$E_{in} = E_{atom} + E_{mol} + E_{slit} + \varepsilon_{loss} \quad \ldots\ldots (1)$$

Approximately 30% of the incident energy E_{in} passes through the slits E_{slit} with most of the remaining energy being absorbed by the grating material. There is insufficient energy to cause electrons to migrate to new orbitals and thus most of the absorbed energy ends up as increased molecular activity. It should be noted that incident energy is mainly comprised of kinetic energy but in some cases (C60 fullerenes) there is significant thermal energy present.

Diffraction gratings are typically manufactured from silicon nitride wafers that have been precisely engineered with nanometer wide slits. Five of the six experiments used SiNx gratings and the sixth used a gold plated SiNx grating.

If a thin slab of wafer material without any slits is placed in the path of an incident beam, then internally in the wafer there will be increased vibrational activity (neglecting rotational and translational modes) which can be thought of as an increase in phonon excitation. In the slitless slab phonons propagate freely throughout the wafer with little or no external effects being observed.

When slits are introduced into the wafer, potential wells are created by the air gaps and many degrees of freedom are removed from phonon propagation with a resulting accumulation of energy around the slits. It is postulated that the higher energy levels around the slits leads to the emission of infrared radiation. Alternatively stated, the presence of diffraction slits in the wafer initiates a phonon to photon conversion process and infrared radiation is emitted.

This radiation is quantized as original phonon activity was quantized and the wavelength of the infrared radiation will be the characteristic spectral emissivity wavelength ,λ_e, of the grating material.

Henceforth this radiation will be referred to as QEM radiation or QEM fields. It has been shown [8] that the spectral emissivity wavelength for SiNx is 8.3 microns and for gold

[9] the emissivity wavelength is 20.5 microns. For single slit experiments weaker QEM fields are expected as phonon propagation is less restricted.
Having established the source of the QEM fields and their wavelengths, field equations can now be formulated with the intention of demonstrating that weak QEM fields can introduce microscopic curvature in local spacetime.

II. THE FIELD EQUATIONS

Einstein Field Equations (EFE) were developed in the context of cosmological distances and massive extraterrestrial objects but there is a growing realization that the field equations can also be applied microscopically to local spacetime yielding accurate predictions. QEM fields are therefore framed in this manner with the well known equation relating energy density to curvature.

$$R_{ab} - \frac{1}{2} g_{ab} R = \frac{8\pi G}{c^4} T_{ab} \qquad \text{..... (2)}$$

Given a pseudo Riemannian manifold [M, g] with g_{ab} being a solution to the above equation, if discussions are limited to electrovac spacetimes in which the stress energy tensor, T_{ab}, is derived from source-free, massless electromagnetic fields such as the QEM fields previously described, then it can be easily shown that in these cases T_{ab} is traceless and the field equation reduces to:

$$R_{ab} = \frac{8\pi G}{c^4} T_{ab} \qquad \text{..... (3)}$$

where R_{ab} is the Ricci curvature tensor. $[R_{ab}] = m^{-2}$

It should be noted that in this analysis all physical constants are retained and the following nomenclature [Kg], [m], [s] ,[C] , [A] is used for dimensional units.

Cylindrical coordinates are best suited to slit experiments with the z-axis being along the height of the slit. Exact solutions to the field equations exist [1] for a stationary,, cylindrically symmetric, electrovac spacetime with Killing vectors $[\varphi, 0, \eta, 0]$ ($\varphi = \partial_t$ and $\eta = \partial_\upsilon$).. A general line metric with time independent components (stationary) in the Weyl-Lewis-Papapetrou format [1] can be written with signature [-,+,+,+]

$$ds^2 = -fc^2dt^2 + 2\omega f d\theta c dt + \frac{e^{2u}}{f} dr^2 + (\frac{r^2}{f} - \omega^2 f) d\theta^2 + \frac{e^{2u}}{f} dz^2 \qquad \text{..... (4)}$$

where the coordinate system is [ct,r,θ,z]

The metric tensor can then be written in component form as:

$$g_{ab} = \begin{pmatrix} -f & 0 & \omega f & 0 \\ 0 & \frac{e^{2u}}{f} & 0 & 0 \\ \omega f & 0 & (\frac{r^2}{f} - \omega^2 f) & 0 \\ 0 & 0 & 0 & \frac{e^{2u}}{f} \end{pmatrix} \qquad \text{..... (5)}$$

both f(r) and u(r) are functions of r only and in the general case ω is also a function of r. Symmetry considerations suggest the following properties for the electric and magnetic fields under study.

(a) The electric field is purely radial – E_υ , E_z are zero
(b) The radial component E_r is a function of r only
(c) B_z is the only non-zero component of the magnetic field
(d) B_z is a function of r only.
The electromagnetic vector potential of such a field, A_a, can be written as

$$A_a = [A_t, 0, A_\upsilon, 0] \qquad \text{..... (6)}$$

which shares the symmetry of the Killing vector $[\zeta, 0, \eta, 0]$ and $A_t = P(r)$, $A_\upsilon = Q(r)$ are functions of r only. The electromagnetic field tensor F_{ab} can be derived from the vector potential as:

$$F_{ab} = \nabla;_a A_b - \nabla;_b A_a \qquad \text{..... (7)}$$

Because of symmetries in the Christoffel connections, the covariant derivates in (7) reduce to partial derivates then:

$$F_{ab} = \partial,_a A_b - \partial,_b A_a \qquad \text{..... (8)}$$

$$F_{ab} = \partial_a A_b - \partial_b A_a \qquad \text{..... (8)}$$

The non-zero components of F_{ab} are

$F_{01} = -P'(r)$ $F_{12} = Q'(r)$
$F_{10} = P'(r)$ $F_{21} = -Q'(r)$

where the prime ' denotes differentiation with respect to r.

For the QEM fields under study, the anti-symmetric electromagnetic field tensor Fab can be written in general component form as:

$$F_{ab} = \begin{pmatrix} 0 & -P'(r) & 0 & 0 \\ P'(r) & 0 & Q'(r) & 0 \\ 0 & -Q'(r) & 0 & 0 \\ 0 & 0 & 0 & 0 \end{pmatrix} \qquad \text{..... (9)}$$

P'(r) is the radial component of the electric field intensity E/c with units $[KgC^{-1}s^{-1}]$ and Q'(r) is the z-component of the magnetic flux density B with units $[KgA^{-1}s^{-2}]$ or [Tesla]

Using the Einstein-Hilbert Lagrangian approach, the Einstein Maxwell equations with vanishing electromagnetic sources [3] [6] can be written as:

$$T_{ab} = \varepsilon_0 c^2 \left[\frac{1}{4} F_{ab} F^{ba} g_{ab} - F_{ac} F_b{}^c \right] \qquad \text{..... (10)}$$

Solutions to eq (3) and (10) with the fields as described in eq (9) are known as electrovac solutions. If the fields satisfy $F_{ab}F^{ba} \neq 0$ everywhere in local spacetime then the spacetime is said to be a non-null electrovacuum [3]. It will be shown later that the fields are indeed non-null and that the Rainich algebraic conditions are met [3] [4] thereby ensuring that the chosen metric is truly an electrovac solution and that g_{ab} is necessarily a solution to eq (2) and fully describes the fields in local space time.
Specific electrovac solutions relevant to the local spacetime of slit experiments are now examined. Expressions for the components of the general metric eq (5) namely f, u and ω are sought such that eq (3) and eq (10) are satisfied along

with the non-nullity conditions and the Rainich algebraic conditions. Expressions for P'(r) and Q'(r) in terms of the metric components are also required.

III.SOLUTIONS TO THE FIELD EQUATIONS

In 1983 Van den Bergh and Wils (VDB) provided exact solutions [2],[5],[7] for non-null electromagnetic fields in a stationary, cylindrically symmetric, electrovac spacetime. Their solutions were derived from the general electrovac metric eq (4).

They found three families of solutions the first of which is applicable to this analysis. Using the notation from eq (4) and (5), the VDB solution is:

$$f(r) = k^2 \sec^2(ks\ln(ar)) \qquad \text{..... (11)}$$

$$u'(r) = \frac{1}{4}\frac{r}{f^2} f'^2 - \frac{r}{f}\left(\frac{sf}{r}\right)^2 \qquad \text{..... (12)}$$

It should be noted that the VDB solution introduces three new arbitrary constants k, s, and a into the metric which need to be rationalized and brought into the microscopic framework of slit experiments. Additionally the metric component ω has to be discussed.

By inspection of eq (4) it is clear that both u(r) and f(r) are dimensionless while ω has units of [m] and from eq (11) the constants 'k' and 's' are dimensionless while 'a' has units of $[m]^{-1}$

There is some disagreement in the literature as to exactly what constitutes a static field.. The VDB position is that ω = *constant* ;ω' = 0 defines a static field, other authors require ω = *0* for static fields. Our equations reflect the VDB position and the QEM fields are therefore considered to be static with constant ω. The exact value of ω will be determined later.

The VDB solution also provides equations for the electric and magnetic fields:

$$P(r) = \omega k \tan(ks\ln(ar))\frac{E}{c} \qquad \text{..... (13)}$$

$$P'(r) = \omega s \frac{f(r)}{r}\frac{E}{c} \qquad \text{..... (14)}$$

$$Q'(r) = -\omega s \frac{f(r)}{r} B \qquad \text{..... (15)}$$

To preserve dimensional accuracy, unit electric and magnetic fields were inserted into the VDB expressions yielding the above equations where E is the unit electric field intensity of magnitude 1 and units $[KgC^{-1}ms^{-2}]$ similarly B is the unit magnetic flux density with magnitude 1 and units $[KgA^{-1}s^{-2}]$ and c is the speed of light in a vacuum

The differential equation (12) can be easily solved by direct substitution yielding:

$$u(r) = -k^2 s^2 \ln(ar) \qquad \text{..... (16)}$$

where 'a' is the constant of integration. The term e^{2u} in the metric then becomes:

$$e^{2u} = e^{-2k^2 s^2 \ln(ar)} = (ar)^{-2k^2 s^2} \qquad \text{..... (17)}$$

With equations (11) through (17) in hand, the metric and its inverse can be written in terms of k, s, a and similarly F_{ab}, F^{ba} and T_{ab} can be obtained in terms of k, s, a. The resulting expressions are long and complex and were obtained with the assistance of a Computer Algebra System (CAS)

(IVa) THE EXTENT OF LOCAL SPACETIME

Local spacetime is defined in terms of its coordinates as:

$$\begin{aligned} q_r <= r <= 10 \text{ mm} \\ 0 <= \upsilon <= \pi \\ -500 \text{ mm} <= z <= 500 \text{ mm} \end{aligned} \qquad \text{..... (18)}$$

Since local spacetime is defined as a source-free electrovacuum its r-coordinate cannot include the diffraction grating. Local spacetime is then defined to begin at a distance q_r away from the grating. In this analysis q_r is chosen as 10 nanometers. Other small values could also have been chosen.

Examination of eq (4) and (11) shows that coordinate singularities are possible at r-values where ksln(ar) is a multiple of π/2 and f(r) becomes indeterminate. Since there are no singularities in local spacetime the quantity ksln(ar) must be chosen to be less than π/2.

'a' is one of the arbitrary constants of the VDB metric and theory suggests that it is the reciprocal of the characteristic spectral emissivity wavelength ,λ_e, of the grating material. Appropriate limits for $\lambda_e$are 1 micron to 100 microns. The limits for 'ar' and 'ks' can then be determined as:

$$10^{-4} <= ar <= 10^{+4}$$

and neglecting negative values of ks:

$$0 < ks < 0.17 \qquad \text{..... (19)}$$

Typically ks is in the range of 0.05 to 0.03 avoiding any coordinate singularities.

(IVb) NON-NULLITY

After simplification, the following expression is obtained

$$F_{ab}F^{ba} = 2P'(r)^2 (ar)^{2k^2 s^2} \qquad \text{..... (20)}$$

By definition k, s, a are non-zero and therefore eq (20) is non-zero wherever the electric field P'(r) exists and r>0 which is precisely the definition of local spacetime. Therefore the non-nullity conditions in [3] are satisfied.

(IVc) RAINICH CONDITIONS

Long ago Rainich developed [3],[4] three algebraic conditions to ensure that a chosen metric solution was indeed an electrovac solution to the EFE. His algebraic conditions apply to the stress energy tensor in the following manner:

1. Trace of $T_{ab} = 0$
2. The energy density $T_{00} >= 0$
3. $T_{au}T^{u}_{b} = (1/4)(T_{vw}T^{wv})g_{ab}$

where u, v, w are dummy indices and g_{ab} is the metric under test. When these conditions are applied to the VDB metric the following results:

(a) As expected, the CAS computes the trace of T_{ab} as zero.

(b) The expression for energy density T_{00} is computed as:

$$T_{00}(r)=\frac{\varepsilon_0 (ks)^2 k^4 (ar)^{2k^2s^2}}{2r^2\cos^6(ks\ln(ar))}\omega^2E^2 \quad \text{J/m3} \quad \text{..... (21)}$$

where ω=1 and E =1. All exponents in eq (21) are even numbers therefore T_{00} must be >=0 and Rainich No 2 is satisfied.

(c) Each of the sixteen components of the tensor equation (condition No 3 above) was evaluated using the CAS. Both sides of the identity were evaluated and checked for equality. A typical evaluation for the (0,0) component is:

$$T_{au}T^{u}{}_{b}(0,0)=\frac{{\varepsilon_0}^2 k^6 (ks)^4 (ar)^{4k^2s^2}}{4r^4\cos^{10}(ks\ln(ar))}\omega^4E^4 \quad \text{..... (22)}$$

The RHS $(1/4)(T_{vw}T^{wv})g_{ab}(0,0)$ evaluates to exactly the same expression as eq (22). The CAS script checked all components and equality was found in each case. Therefore Rainich No 3 is satisfied.

(IVd) KRETSCHMANN INVARIANT

The Ricci curvature scalar R vanishes by definition in eq (3) so another invariant scalar needs to be evaluated as a test for curvature in local spacetime. The Kretschmann scalar which is also derived from the Riemann curvature tensor is used for this purpose. The CAS was used to evaluate Kr and after simplification yields:

$$K_r=R_{abcd}R^{abcd}=\frac{8k^4(ks)^4(ar)^{4k^2s^2}}{r^4\cos^8(ks\ln(ar))} \quad \text{..... (23)}$$

Which is non-vanishing if r>0 establishing that weak QEM fields can introduce curvature in microscopic spacetime.

(IVe) PHYSICAL INTERPRETATION OF THE METRIC CONSTANTS.

The metric solution describing QEM fields and their behaviour – namely eq (4), eq(10) and eq(11) through (17) have been reduced to a system of equations involving four constants (k,s,a,ω). Physical interpretation of these constants will now be offered. Theory suggests and experimental verification confirms the following:

k : As discussed earlier, molecular vibrations in the grating material leads to quantized fields and each configuration of those fields is represented by a unique k-value thus k represents the field configuration and is also the order of diffraction holding values of (0, ±1,±2, ±3…±n).

s : A scale factor that tunes the metric solution to the microscopic world of slit experiments. The constant 's' allows equations that were written for planets and stars and distances of light years to operate at the nanometer scale with masses of the order of 10^{-24} Kg.

a : The constant 'a' is the reciprocal of the characteristic spectral emissivity wavelength ,λ_e, of the grating material

ω : The constant ω can be thought of as the twist factor of the QEM fields. A constant ω implies that there is no twist and that the fields are static ; ω= 1 is chosen so that the electric and magnetic fields have the same magnitude.

ks: The actual scale factor used in the equations is 'ks' – the product of 'k' and 's'. 'ks' plays a pivotal role in setting the environment for the equations of motion and the equations of particle diffraction. Jumping ahead slightly we now present an equation derived from particle deflection theory

$$\frac{\cos^2(Aks)}{ks}-B=0 \quad \text{..... (24)}$$

where $A=\ln(7q_r/\lambda_e)$ and $B=d\ln(6)/q_r$.

The transcendental equation can be readily solved numerically and yields solutions accurate to 0.4%. In eq (24) q_r and λ_e are as previously defined and d is the period of the diffraction grating. It should be noted that ks is a function of (λ_e , d, q_r) and is not dependent on particle parameters such as velocity or mass and neither is it dependent on slit width. ks essentially describes the environment of the slit experiment – the grating material, the periodicity of the slits and the start of local spacetime.

IV.EQUATIONS OF MOTION

Equations of motion for massive, uncharged test particles in the QEM fields are now presented. Similar equations for charged particles and the massless photon are yet to be derived. Using the methods of Carroll [10] equations of motion for non-null fields can be developed purely from the metric and the symmetry of the Killing vectors.

The timelike Killing vector $\xi^u=(\partial_t)^u=(1,0,0,0)$ and its covariant form $\xi_u=g_{ab}\xi^u=(-f,0,\omega f,0)$ are easily obtained from symmetry considerations. Along geodesics, energy is the conserved quantity of the timelike Killing vector and noting that E is energy per unit mass [m^2s^{-2}] and the signature is [-+++] the following is obtained with τ being the affine parameter:

$$\frac{E}{c}=-\xi_u\frac{dx^u}{d\tau} \quad \text{..... (25)}$$

and with $x^0=ct$

$$\frac{E}{c}=cf\frac{dt}{d\tau}-\omega f\frac{d\theta}{d\tau} \quad \text{..... (26)}$$

The spacelike Killing vector $\eta^u=(\partial_\theta)^u=(0,0,1,0)$ and its covariant $\eta_u=g_{ab}\eta^u=[\omega f,0,(\frac{r^2}{f}-\omega^2 f),0]$ are similarly obtained. Along geodesics, angular momentum is the conserved quantity of the spacelike Killing vector and noting that L is the magnitude of the angular momentum vector per unit mass [m^2s^{-1}] then:

$$L=\eta_u\frac{dx^u}{d\tau} \quad \text{..... (27)}$$

$$L=\omega fc\frac{dt}{d\tau}+\left(\frac{r^2}{f}-\omega^2 f\right)\frac{d\theta}{d\tau} \quad \text{..... (28)}$$

Substituting dt/dτ from eq (26) into (28) yields:

$$\frac{d\theta}{d\tau}=\frac{bf}{r^2} \quad \text{..... (29)}$$

and $b=(L-\omega E/c)$ [m^2s^{-1}] ..... (30)

An equation for dθ/dr is necessary for particle trajectory prediction. An expression for dr/dτ is first obtained from the geodesic equation and then combined with eq (29) to arrive at

dθ/dr. The well known geodesic equation for massive particles is:

$$g_{ab}\frac{dx^a}{d\tau}\cdot\frac{dx^b}{d\tau}=c^2 \qquad \text{..... (31)}$$

Noting that motion occurs in the r-θ plane so that dz/dτ= 0 the following is obtained:

$$\left(\frac{dr}{d\tau}\right)^2=\frac{b^2f^2}{e^{2u}}\left[\frac{1}{r_0(r)^2}-\frac{1}{r^2}\right] \quad [m^2s^{-2}]$$

$$r_0(r)^2=\frac{b^2f^2(r)}{c^2f(r)+E^2/c^2} \quad [m^2] \text{ ..... (32)}$$

The desired equation for dθ/dr can now be written:

$$\frac{d\theta}{dr}=\frac{(ar)^{-k^2s^2}r_0(r)}{\sqrt{r^4-r^2r_0(r)^2}} \qquad \text{..... (33)}$$

To obtain the particle trajectory θ(r), eq (33) needs to be integrated with eq (32), (30) and (11) included in the integrand. To date a closed form analytical solution to eq (33) has not been found. However numerical integration of the full equation set is possible and accurate values of θ(r) can be obtained at desired r-values.. When eq (33) is rewritten as :

$$\frac{d\theta}{dr}=\left(\frac{1}{r^2}\right)\frac{(ar)^{-k^2s^2}r_0(r)}{\sqrt{1-\frac{r_0{}^2(r)}{r^2}}}=\frac{1}{r^2}K(r) \qquad \text{..... (34)}$$

then K(r) is observed to be almost a constant, prompting the following:

$$\theta(r)\approx-\frac{K(r)}{r}+\theta_K \qquad \text{..... (35)}$$

Numerical integration results suggest that such a model is accurate. The term -K(r)/r is the transient response in r-space. When the particle has traveled 100 nanometers from the grating θ(r) has achieved 90% of its final value and at 10 microns it has achieved 99.9%. The transient response has little or no effect after r>100 nm and therefore the steady state response can be written exactly as:

$$\theta(r)=\pm\theta_K \qquad \text{..... (36)}$$

Numerical integration results confirm that θ(r) always reaches an asymptotic value and that no other variations occur after. The ± sign originates from the square root in eq (33).

Equation (36) represents a ray-like trajectory in the r-θ plane (polar cords) and θ_K is the angle of deflection. The transient response introduces a slight curvature at the start of the ray when r< 100nm. The equations of motion clearly show that QEM fields will introduce microscopic curvature and that curvature is manifested as ray-like deflections.

(Va) IMPACT PARAMETER & THE θ_K MODEL

The quantity, b, in eq (30) is a general impact parameter which describes the initial conditions per unit mass of test particles entering a field of radiation. A specific impact parameter has to be developed for slit-type particle diffraction.

After numerous simulations it became apparent that to achieve deflection angles similar to what is reported in the literature, the parameter 'b' had to be inversely proportional to the momentum of the particle.

$$b=\frac{D}{mv_i} \quad [m^2s^{-1}] \qquad \text{..... (37)}$$

which meant that [D] should have units of [Kg m^2 s^{-1} m s^{-1}].. Planck's constant and the speed of light provided the correct units. Noting that the particles position in the slit contributes to the angular momentum, the following could be written.

$$b=ks\ln\left(\frac{3d}{q_s}\right)\frac{hc}{mv_i} \qquad \text{..... (38)}$$

The impact parameter eq (38) yields excellent predictive results when combined with the other equations. Numerical integration solutions for θ(r) eq (33) using eq (38), (32) and (11) in the integrand yield expected values of deflection angles for many dozens of simulations tested.

In eq (38) ks, d and c are as previously defined with h being Planck's constant, m the mass of the particle, v_i being the velocity of the particle (assumed constant) and q_s is a new quantity representing the particles position in the slit. q_s is measured from the center of a neighboring bar to the center of the particle. In this way the central path trajectory is defined to always be d/2 regardless of grating geometry. The edges of the slits are then given by:

$$q_s=\frac{d}{2}\pm\frac{u}{2} \text{ where u = slit width} \qquad \text{..... (39)}$$

With eq (38) in hand, a model equation for θ_K was formulated using inputs from eq (38) and eq (11).

$$\theta_K=\ln\left(\frac{3d}{q_s}\right)\frac{hk}{mv_iq_r}(ks)\sec^2(ks\ln(\frac{8q_r}{\lambda_e})) \text{ ... (40)}$$

Although there is no closed form solution to eq (33) we now have an exact steady state response eq (36) and an accurate model equation (40) for θ_K. The model equation has been tested over a wide range of simulations with varying values of ks, d, q_s, m, vi and λ_e. In all cases θ_{MODEL} was in good agreement with $\theta_{NUMI.}$ The average error was 0.75%. Model (40) computations have been used in experimental verification.

It is interesting to note that when a particle takes the central path through the slit, the deflection angle is the same as the de Broglie deflection. The de Broglie deflection angle is really the central path deflection where ln(3d/q_s) reduces to ln(6). Deflection angles will vary with particle path position and those path dependent deflection angles can be predicted by eq (33) , (40) allowing random distributions to be introduced.

V. PARTICLE DIFFRACTION

Particle diffraction is quite different from wave diffraction in that particles travel in straight lines (ray-like trajectories) and other than collisions there is no interference between particles during flight time For ease of notation we can consider a typical experiment in Cartesian coordinates where the particles travel in the y-direction, the height of the slits is in the z-direction and the width of the grating is in the x-direction.

QEM fields of radiation are associated with each slit and those fields introduce curvature in the microscopic spacetime near the slit. That curvature manifests itself as particle deflection and at any time, t, the QEM fields can be in any

one of the finite number of configuration states (k-value states). There is nothing in the theory to suggest that neighboring slits will be in the same configuration state, to the contrary, the configuration state of individual slits is a purely random event dependent on molecular vibrations.

What is not random, however, is the angle of deflection θ_K associated with the k^{th} field configuration which is given deterministically by eq (33) and (40). We can envisage particles arriving at the detector in a seemingly random manner but actually they are following the dictates of molecular vibrations and eq (33), (40).

In the case of a double slit experiment if, by chance, both slits are in the same configuration state then deflected particles will arrive at the detector on parallel paths that are d nanometers apart, where d is the distance between slit centers (typically100 nm). In most experiments the active detector area (the area where counting takes place) has a width of approximately 10 mm. Clearly on the detector width scale a 100 nm spacing will appear to be coincident – the two 'hits' will appear to be one.

Generally, in particle diffraction, parallel paths are coincident, under allowable limits. The allowable limits are that the spacing between the paths must be much smaller than the active detector width.

In the case of multi-slits, the incident beam from the collimator will illuminate N slits (N≈100), then the spacing between parallel paths emerging from slits at either end of the illumination will be $O(10^{-5})$ which is 1000 times smaller than the active width and parallel paths will also appear to be coincident in multi-slit cases. In other words multi-slit gratings do not add any new maxima to the diffraction pattern; they add intensity to the pattern. If a double slit experiment had an intensity of I on some intensity scale then a multi-slit grating with N illuminated slits will have an intensity of:

$$I_{multi} = I_{dbl}\left(\frac{N}{2}\right) \qquad \text{..... (41)}$$

VI. PROBABILITY AMPLITUDES

In slit experiments, the intensity at a given angle of deflection is measured as the number of particles impacting the detector per unit time at that deflection angle.. Therefore the intensity of the k^{th} maxima is the number of particles arriving at the detector with deflection angle = θ_K It has been shown that the k^{th} angle of deflection θ_K is directly related to the k^{th} configuration state eq (33), (40). It follows then that the intensity I(k) of the k^{th} maximum is directly proportional to the probability P(k) of finding the fields in the k^{th} configuration state.

$$I(k) = IyP(k) \qquad \text{..... (42)}$$

where Iy is a constant to be determined.

The probability of finding the fields in the k^{th} configuration state is known to be the square of the modulus of the complex-valued probability amplitude a(k) and for real-valued a(k):

$$P(k) = a^2(k) \qquad \text{..... (43)}$$

As will be shown, the probability amplitudes can be derived from the wave function in configuration space.

For the electromagnetic fields as described by eq (9), (14) and (15) the wave function $\psi(r_n)$ in r_n space is the convolution of two descriptors $f(r_n)$ and $g(r_n)$ where r_n is the dimensionless, normalized r-coordinate

$$r_n = \frac{r}{q_r} \qquad \text{..... (44)}$$

and
$$f(r_n) = B_0 \quad \text{for } -\beta \le r_n \le \beta \qquad \text{..... (45)}$$
$$= 0 \quad \text{otherwise.}$$

$f(r_n)$ is a rectangular pulse of width 2β which implies that the wave function is partly a standing wave of amplitude B_0.

and
$$g(r_n) = \frac{1}{r_n^{\,2} + \alpha^2} \qquad \text{..... (46)}$$

$g(r_n)$ is related to the energy density of the configurations.

then
$$\Psi(r_n) = f(r_n) * g(r_n) \qquad \text{..... (47)}$$

where * is the convolution operator.

Theory suggests that the probability amplitudes a(k) are given by the Fourier transform of $\psi(r_n)$ to k-space, then,

$$a(k) = \mathsf{F}\,(\psi(r_n)) \qquad \text{..... (48)}$$

By the convolution theorem,

$$\mathsf{F}(\psi(r_n)) = \mathsf{F}(f(r_n))\ \mathsf{F}\,(g(r_n)) \text{..... (49)}$$

Each Fourier transform will be evaluated separately so that the amplitudes a(k) can be determined.

$$\mathsf{F}\,(f(r_n)) = \int_{-\infty}^{+\infty} B_0 e^{-ikr_n}\,dr_n = \int_{-\beta}^{+\beta} B_0 e^{-ikr_n}\,dr_n \text{ ... (50)}$$

$$= \frac{2B_0}{k}\left(\frac{e^{ik\beta} - e^{-ik\beta}}{2i}\right) \text{which by Euler's identity is}$$

$$\mathsf{F}\,(f(r_n)) = 2\beta B_0\,\frac{Sin(k\beta)}{k\beta} \qquad \text{..... (51)}$$

$$\mathsf{F}\,(g(r_n)) = \int_{-\infty}^{+\infty} \frac{1}{(r_n^{\,2} + \alpha^2)} e^{-ikr_n}\,dr_n = \frac{\pi}{\alpha} e^{-\alpha|k|} \text{ .. (52)}$$

From eq (48), (49) the probability amplitudes can now be written as:

$$a(k) = \frac{2\pi\beta B_0}{\alpha}\,\frac{Sin(k\beta)}{k\beta}\,e^{-\alpha|k|} \qquad \text{..... (53)}$$

And from eq (43) the probability of finding the fields in the k^{th} configuration is given by:

$$P(k) = \frac{4\beta^2 B_0^{\,2}\pi^2}{\alpha^2}\,\frac{Sin^2(k\beta)}{k^2\beta^2}\,e^{-2\alpha|k|} \text{ ..... (54)}$$

The constant B_0 is chosen so that $\sum_{k=1}^{n} P(k) = 1$

From eq (41) and (42), it follows that

$$I(k) = \frac{2NI_y\beta^2 B_0^{\,2}\pi^2}{\alpha^2}\,\frac{Sin^2(k\beta)}{k^2\beta^2}\,e^{-2\alpha|k|} \text{ ..... (55)}$$

But $\underset{k\to 0}{Lim}\left(\frac{Sin^2(k\beta)}{k^2\beta^2}\right)=1$ and $\underset{k\to 0}{Lim}\left(e^{-2\alpha|k|}\right)=1$

therefore $$I(0)=\frac{2NI_y\beta^2{B_0}^2\pi^2}{\alpha^2} \quad \text{..... (56)}$$

which allows the above group of constants to be determined from the experimentally measured value of the zeroth order peak intensity. The higher order peak intensities can be computed relative to I(0) as:

$$\frac{I(k)}{I(0)}=\frac{Sin^2(k\beta)}{k^2\beta^2}e^{-2\alpha|k|} \quad \text{..... (57)}$$

This methodology and eq (57) has been used in experimental verification.

The function $\frac{Sin(k\beta)}{k\beta}$ is also known as Sinc(kβ) and it can be considered as a sampling function that provides peak intensities. In other applications (bandwidth filter design) the Sinc function is sampled in units of time to obtain filter response here the Sinc function is sampled in units of 'k' to obtain peak intensities.

The angular frequency, β, of the sampling function is the most important factor in determining the appearance of the diffraction pattern – which peaks are high or low. The other factor in determining peak intensities is the damping exponent, α. It should be noted that the derivation of F *(g(r$_n$))* requires that α be positive (α>0). The damping factor $e^{-2\alpha|k|}$ ensures that higher order peaks have lower intensities and |k| ensures pattern symmetry.

(VIIa) THE ANGULAR FREQUENCY β

When the fields are evaluated at $(1+\beta)q_r$ which is the center of the standing wave pulse eq (45), the following expression has been found to be invariant across the six experiments:

$$\frac{(ks)(\frac{d}{q_r})\ln(6)(\frac{q_r}{\lambda_e})^{2k^2s^2}}{Cos^2(ks\ln(\frac{q_r}{\lambda_e}(1+\beta)))}=1 \quad \text{..... (58)}$$

An expression for β can be obtained from eq (58) as follows:

$$1+\beta=\left(\frac{\lambda_e}{q_r}\right)e^{-\frac{1}{ks}Cos^{-1}(F)} \quad \text{..... (59)}$$

where $F=\sqrt{(ks)(\frac{d}{q_r})\ln(6)(\frac{q_r}{\lambda_e})^{2k^2s^2}}$ ..... (60)

The claim of invariance across experiments in eq (58) is somewhat misleading, in that, for accurate β-values it is necessary to replace ln(6) in eq (58) with $\ln(6)/\varepsilon_b$ where ε_b is a correction factor shown in Table I.

TABLE I	
Experiment Number	ε_b
1	0.99417618
2	1.00368993
3	1.01241537
4	1.01509721
5	1.00417037
6	1.02496715

These experiments are conducted at the nanometer scale with microrad deflection angles hence it is necessary to know the correction factors to O(10^{-7}). The need for a correction factor may result from.

(a) the use of approximate model (40) equation in the derivation of eq (58). Small inaccuracies in the factor, F, eq (60) will be greatly magnified and lead to significant errors in β as F occurs as an exponent in eq (59).

(b) Equation (58) could be correct as written and there could be experimental setup misalignments leading to the correction factors. In any event the correction factor ε_b has been used to compute β-values for experimental verification.

(VIIb) THE DAMPING EXPONENT α

The field descriptor $g(r_n)$ is a dimensionless quantity related to the energy density of the field configurations and from eq (46) :

$$\frac{1}{1+\alpha^2}=\frac{T_x}{T_0} \quad \text{..... (61)}$$

The energy densities T_x and T_0 are the (0,0) component of the stress energy tensor, T_{ab}, given by eq (21).

$$T_x=T_{00}(xq_r)\ x>1 \quad \text{..... (62)}$$

$$T_0=T_{00}(q_r) \quad \text{..... (63)}$$

Equation (61) can be rewritten as:

$$\alpha=\sqrt{\frac{T_0}{T_x}-1} \quad \text{..... (64)}$$

Using eq (21) the ratioT_0/T_x can be simplified to:

$$\frac{T_0}{T_x}=x^{-2(k^2s^2-1)}\frac{Cos^6(ks\ln(\frac{xq_r}{\lambda_e}))}{Cos^6(ks\ln(\frac{q_r}{\lambda_e}))} \quad \text{..... (65)}$$

TABLE II	
Experiment Number	ε_a
1	1.00059356
2	1.00197248
3	1.00320750
4	1.00106068
5	1.01112845
6	1.02242765

It has been determined that

$$x=\left(\frac{u}{4q_r}\right)^{2k^2s^2} \quad \text{..... (66)}$$

is a reasonable fit for α where u is the nominal slit width. However a correction factor ε_a has to be applied as shown in Table II. The correction factor $\varepsilon_a x$ has been used to compute α-values for experimental verification.

In summary, the relative peak intensities

$$\frac{I(k)}{I(0)} = f(k, ks, q_r, \lambda_e, d, u)$$

are a function of the metric constants k,s,a,q_r and the grating geometry (slit width 'u' and grating period 'd').

VII.GAUSSIAN DISTRIBUTIONS

Typically the slit width, u, is much larger O'(70-400) than the particle diameter, v, leading to the particle position within the slit, the variable q_s, being a random variable with a standard, normal Gaussian distribution. In this analysis the single word 'Gaussian' is used instead of the much longer phrase 'standard, normal Gaussian distribution'.

At each peak location given by θ_K a Gaussian is constructed with the mean being the detector position corresponding to angle θ_K. All Gaussians regardless of diffraction order, k, will have the same standard deviation, σ, as particle position within the slit is independent of field configuration.

From standard probability theory, the probability that a random variable, x, will take a value less than or equal to qs is given by:

$$cdf(q_s, \mu, \sigma) = \int_{-\infty}^{q_s} \frac{1}{\sigma\sqrt{2\pi}} e^{\frac{-(x-\mu)^2}{2\sigma^2}} dx \qquad \text{..... (67)}$$

where the mean is μ and σ is the standard deviation. These integrals can only be evaluated by using lookup tables in various math packages and $cdf(q_s,\mu,\sigma)$ is the result of accessing the lookup table. The probability that a random variable will take a value $q_s \pm \Delta q$ is then

$$P(q_S) = \frac{1.2534\sigma}{\Delta q}\left[cdf(q_S + \Delta q, \mu, \sigma) - cdf(q_S - \Delta q_S, \mu, \sigma)\right]$$

..... (68)

In this analysis Δq = 0.1 nanometer

The factor $(1.2534\sigma/\Delta q)$ is necessary to normalize $P(q_s)$ to a maximum value of 1.0. In this way the Gaussian probabilities can be multiplied by the peak probabilities given by eq (57).

From standard Gaussian probability theory the half maximum probability density occurs at x_w where:

$$x_w = \sigma\sqrt{8\ln 2} \quad \text{[nm]} \qquad \text{..... (69)}$$

It has been determined that the half maximum probability of the Gaussians described in eq (68) occur at:

$$x_w = S\frac{u}{d} \qquad \text{[nm]} \qquad \text{..... (70)}$$

where $$S = \frac{1}{130k^2s^2}\sqrt{uvSec^2(\ln(\frac{4d}{u}))} \quad \text{[nm]} \quad \text{.. (71)}$$

and d,u,v are expressed in nanometers not meters. Then

$$\sigma = \frac{Su}{d\sqrt{8\ln 2}} \quad \text{[nm]} \qquad \text{..... (72)}$$

The standard deviation, σ, in terms of (ks,d,u,v) has been used in computing Gaussian probabilities for experimental verification..

(VIIIb) QEM THEORY – GRAPHICAL REPRESENTATION

Before proceeding to experimental verification the full QEM diffraction theory is presented in graphical form as depicted below

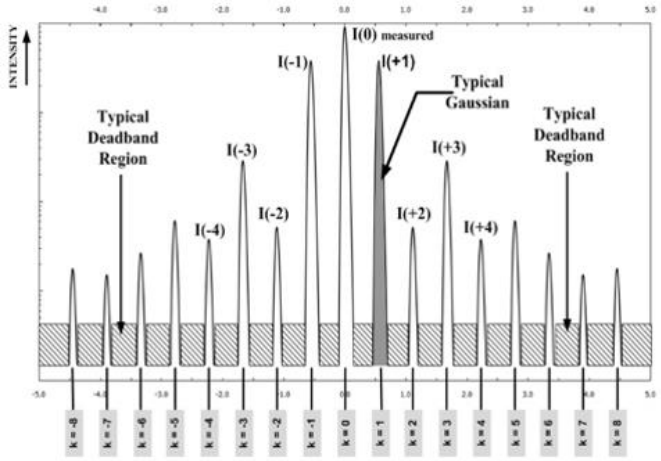

i. The location of the peaks are predicted by eq (33) and (40) and are shown on the x-axis as (k = 0 , k = ±1 , k = ±2 , k = ±3 ….)
ii. The peak intensity of the zeroth order I(0) is a measured value from the experiment
iii. The other peak intensities I(±1) I(±2)) I(±3) …. are given by eq (57) where β is computed from eq (59) , (60) , ε_b and α is computed from eq (64) , (65) , (66) and ε_a
iv. The Gaussian distributions (shaded area) are computed from eq (68) where σ is given by eq (72)
v. The hatched areas between the Gaussians are referred to as deadband regions where presently there is no theoretical probability of finding particles.

Presently the theory assumes that particles either pass through the slit and experience a QEM deflection or that the particles impact the grating material giving up their energy to the molecular structure.

However, in the real world some particles will graze the slit edge and arrive at the detector with a deflection angle a little different from the theoretical value. Slit edge grazing is the main source of deadband activity. Another source of deadband activity, albeit with much lower probabilities, is particle collision whereby particles collide during flight time and arrive at the detector with odd deflection angles.

These deadband activities are not quantified nor are any equations / expressions offered for their flight paths or the probability of their occurrence. Without any formal proof, deadband activity is simulated, in the theoretical plots, by inserting appropriate connecting quadratic segments between the Gaussians.

(VIIIc) VELOCITY SPREAD

Experiments 5 and 6 report significant spread in particle velocity. The theoretical plots for velocity spread consists of a composite plot of the QEM diffraction patterns for the upper and lower velocities. Experimental points are then expected to fall within the area formed by the high and low envelopes. These composite plots are shown in Fig 5b and Fig 6b.

IX. EXPERIMENTAL VERIFICATION

Six experiments from the literature [11],[12],[13] were studied and some important parameters from those experiments are summarized below in Table III. It should be noted that in experiments 1,2,3,4 [11] it was possible to rotate the grating about the z-axis leading to various angles of inclination. This was not possible in experiment 5 [13] or experiment 6 [12].

TABLE III

Experiment Number	1	2	3	4	5	6
Year of Experiment	2000	2000	2000	2000	1988	2003
Type of Particle	Helium Atom	Helium Atom	Helium Atom	Helium Atom	Sodium Atom	C60 Fullerene
Incident Kinetic Energy [milli eV]	65	65	65	65	119	51
Most Probable Velocity [m/sec]	1780	1780	1780	1780	1000	120
Velocity Spread % - FWHM	2.1	2.1	2.1	2.1	12.0	17.0
Particle Mass [Kg] x 10^{-27}	6.646	6.646	6.646	6.646	38.17	1200
Particle Diameter [nanometers]	0.28	0.28	0.28	0.28	0.454	1.10
Grating Material	SiNx	SiNx	SiNx	SiNx	Gold on SiNx	SiNx
Emissivity Wavelength [microns]	8.3	8.3	8.3	8.3	20.5	8.3
Angle of Inclination [degrees]	0	21	27	29	0	0
Grating Period [nanometers]	100	93.3	89.1	87.46	200	100
Slit Width [nanometers]	50	46.68	44.55	43.73	100	55
Distance from Grating to Detector [m]	0.52	0.52	0.52	0.52	1.5	1.2

Following are plots of theoretical predictions (solid line) and experimental results (solid circles) for each of the experiments listed in Table III. For each experiment the values (ks,α,β,σ) are shown.

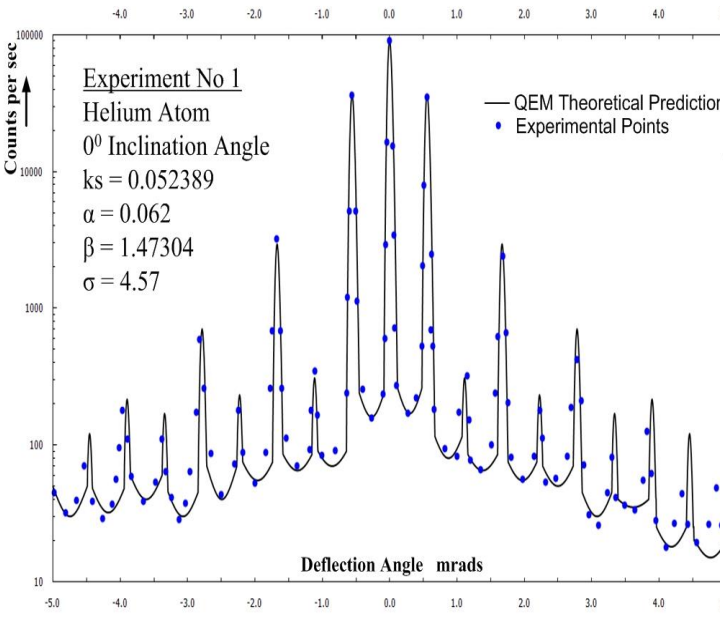

Fig No 1 Helium Diffraction – 0^0 Inclination

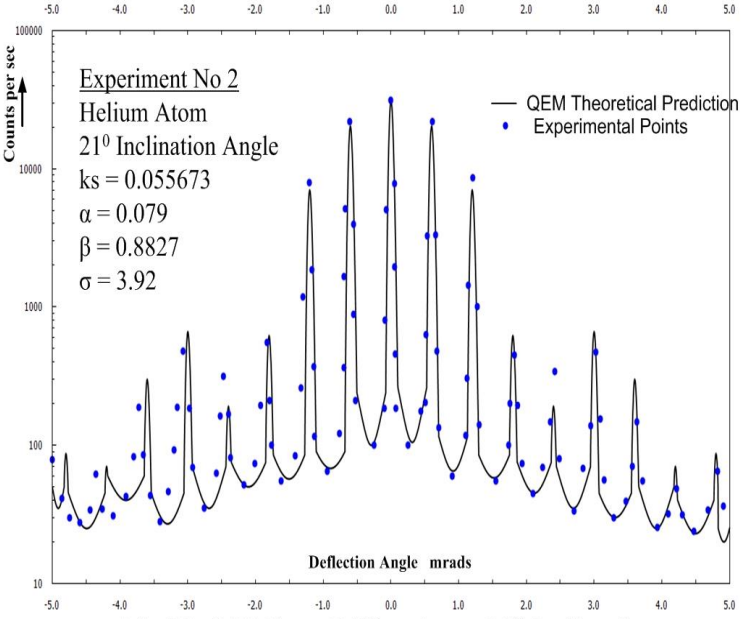

Fig No 2 Helium Diffraction – 21^0 Inclination

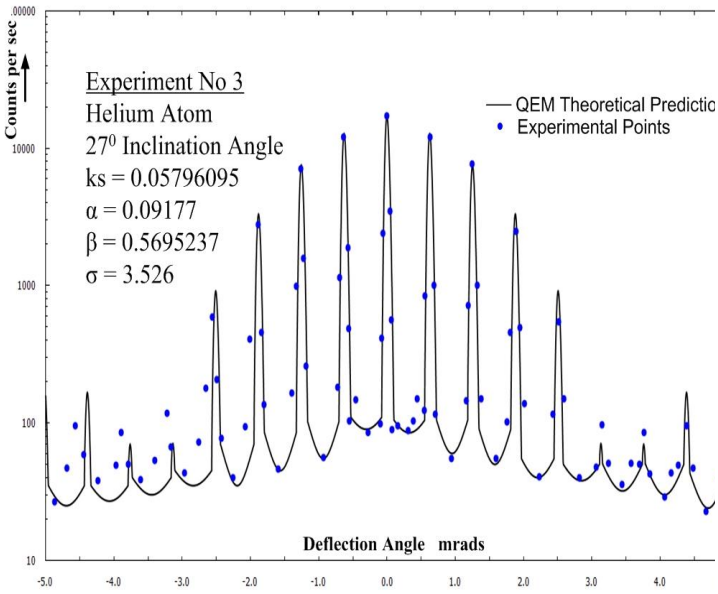

Fig No 3 Helium Diffraction – 27^0 Inclination

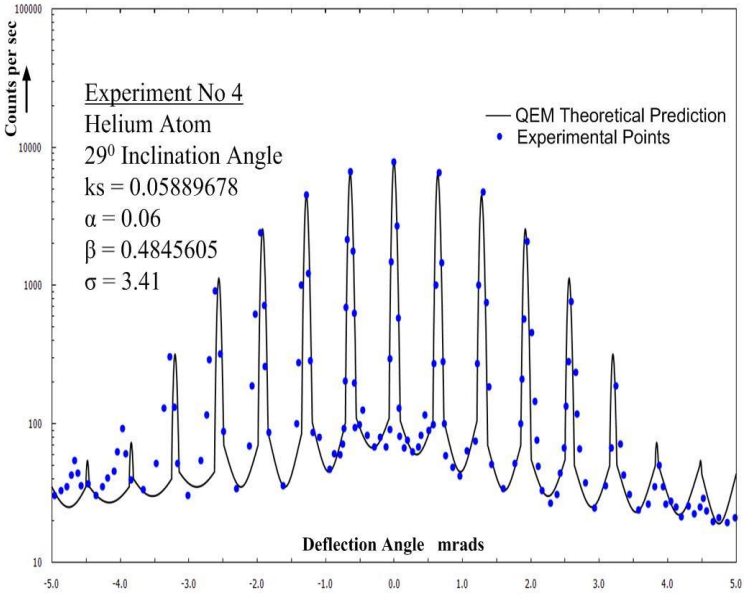

Fig No 4 Helium Diffraction – 29^0 Inclination

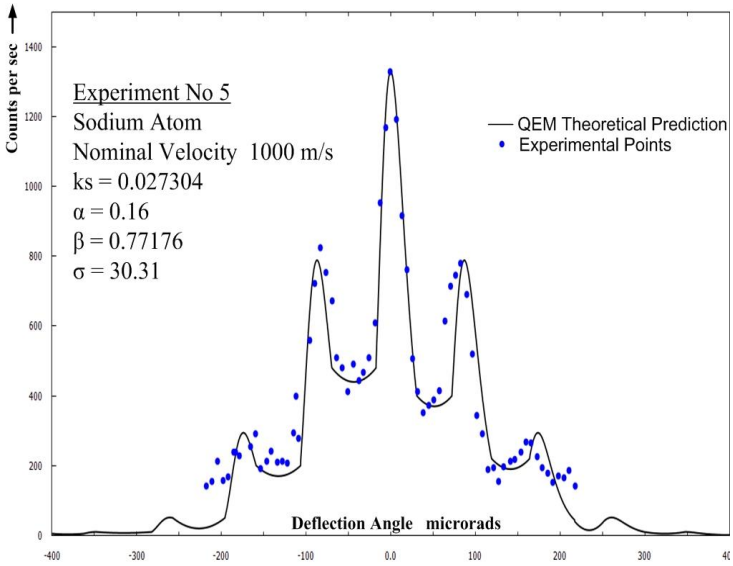

Fig No 5a Sodium Diffraction – Nominal Velocity

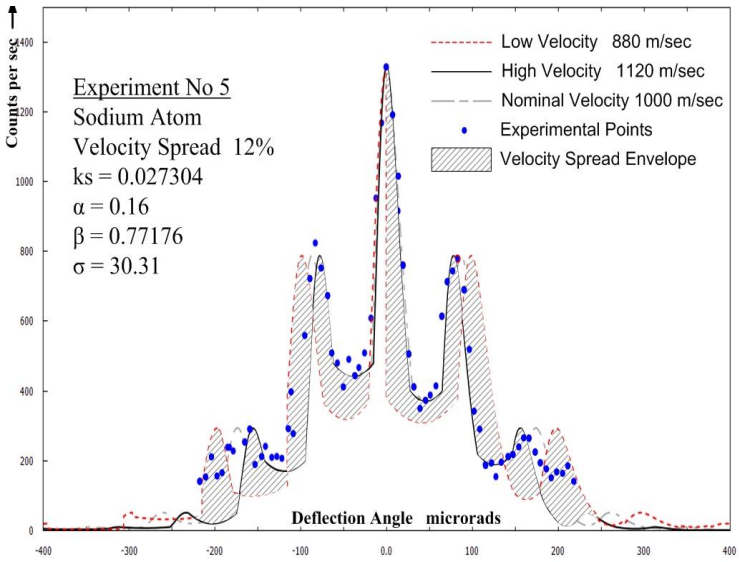

Fig No 5b Sodium Diffraction – Velocity Spread

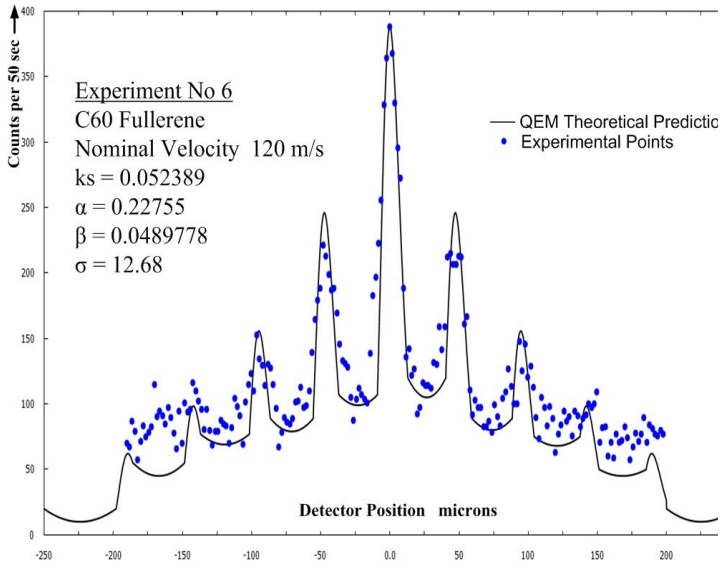

Fig No 6a C60 Fullerene Diffraction – Nominal Velocity

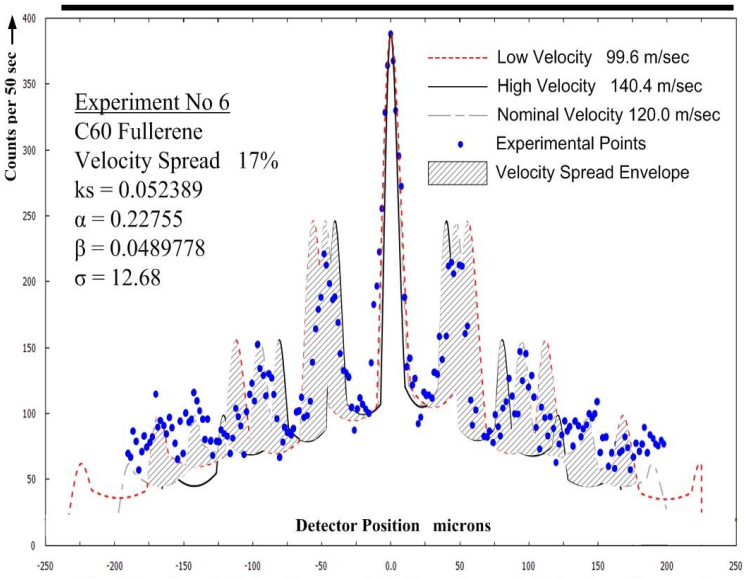

Fig No 6b C60 Fullerene Diffraction – Velocity Spread

The previous plots clearly show that experimental results extracted from the literature are accurately predicted by the new QEM infrared radiation theory. In the case of the helium experiments, the locations, the peak intensities and the Gaussians are all in excellent agreement with experimental results. There are low intensity regions (100 hits per sec or less) where there is divergence between theory and results. This is to be expected as deadband activity is not presently formulated.

In the case of sodium atoms and C60 molecules when velocity spread is factored in, more than 80% of the experimental points fall within the velocity envelope. All told, the QEM theory seems to be aligned with physical measurements.

Characteristic patterns, previously reported in the literature [11] are obtained when normalized intensities, eq (57), are plotted in k-space. We present similar results below to demonstrate that the new theory produces comparable probabilities (intensities) as reported previously.

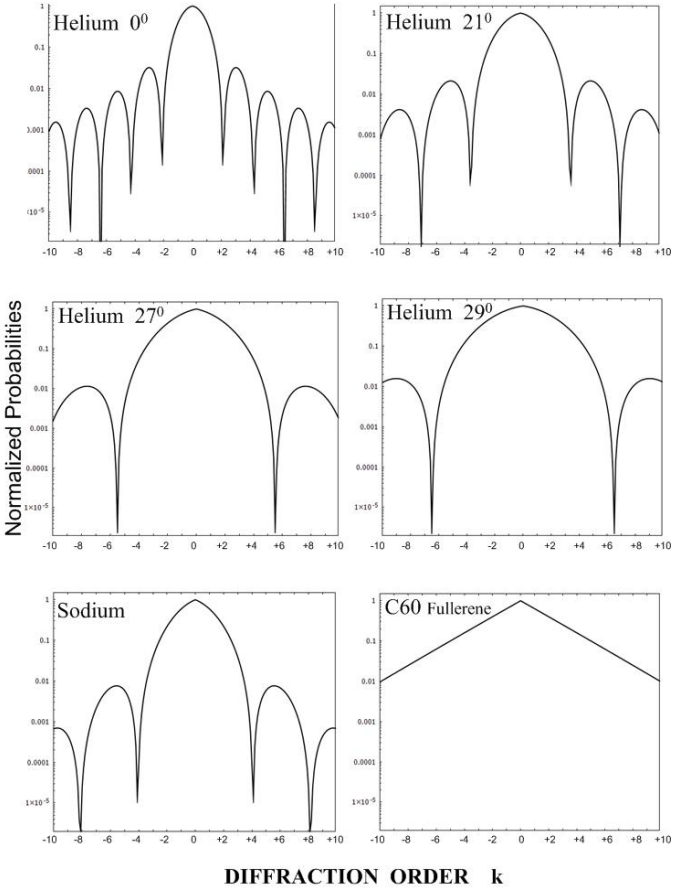

The plot is linear x-axis, logarithmic y-axis. Each experiment has a different β-value and therefore a different Sinc function. The Sinc function is sampled in units of k to obtain the probability that the fields are in configuration k. A multi-peak pattern such as Helium 0^0 will lead to peak intensities that alternate (high to low) with increasing k. While an inverted-v pattern like C60 will lead to peak intensities that decrease almost linearly with k. In the C60 pattern α is predominant while in the other patterns β governs the pattern appearance.

X. CONCLUSIONS

Experimental confirmation of the theorized infrared QEM radiation around diffraction gratings is needed. The author is confident that such radiation will be found.

For years, diffraction patterns in slit experiments have been held up as proof of the wave nature of matter. If this new explanation is correct then one has to reconsider whether matter really has a wave nature and if so, under what conditions are these wave properties exhibited.

Another feature of this analysis is the application of the EFE to microscopic local spacetimes, in this case, the application of source free electrovac solutions to slit experiments. If this theory is proven correct then one must consider writing and solving the field equations within the spacetime of the atom. One can easily theorize that electromagnetic fields generated by the nucleus will introduce significant curvature in atomic spacetime which when coupled with Coulomb attraction can lead to quantized orbits, shells, orbitals. A fresh look at the space within the atom is needed.

ACKNOWLEDGEMENTS

The author would like to thank Prof. Markus Arndt of The Institut fur Experimentalphysik, Universitat Wien, Austria and Prof J. Peter Toennies of The Max Planck Institut fur Stromungsforschung, Gottingen, Germany for providing their experimental results which helped in guiding the development of this work.

REFERENCES

[1] Hans Stephani, Dietrich Kramer, Malcolm Maccallum, "Exact Solutions to Einstein's Field Equations – Second Edition" *Cambridge 2003*

[2] N. Van den Bergh, P.Wils, "A class of stationary Einstein-Maxwell solutions with cylindrical symmetry" *The Institute of Physics 1983*

[3] Charles G. Torre, "The Spacetime Geometry of a Null Electromagnetic Field", *Department of Physics, Utah State University,* Feb 2014

[4] Wytler Cordeiro dos Santos "Introduction to Einstein-Maxwell equations and the Rainich conditions" *Universidade de Brasilia, Brazil, arXiv:1606.08527v1,* June 2016

[5] P.Wils, N. Van den Bergh,"A Case of Dual Interpretation of Einstein-Maxwell Fields" *Universitaire Instelling Antwerpen, Belgium* April 1984.

[6] M. Cermak "Electro-vacuum cylindrical stationary solutions in general relativity" *arXiv:1307.3044v2,* August 2013.

[7] C.B.G. McIntosh "Einstein-Maxwell Space-Times with Symmetries and with Non-Null Electromagnetic Fields" *Monash University, Victoria, Australia,* Dec 1976

[8] Nuggehalli M. Ravindra, SufianAbedrabbo et al, "Temperature-Dependent Emissivity of Silicon-Related Materials and Structures" *New Jersey Institute of Technology Newark, NJ,* July 1997

[9] Telmo Echaniz Ariceta "Infrared spectral emissivity studies on metals and materials for solar thermal applications" *Basque University,* 2016.

[10] Sean M. Carroll "Spacetime and Geometry – An Introduction to General Relativity" *Pearson,* Sept 2003.

[11] R.E. Grisenti, W.Schollkopf, J. P. Toennies "He-atom diffraction from nanostructure transmission gratings: The role of Imperfections" *Max Planck Institut Stromungsforschung,* Feb 2000.

[12] Olaf Nairz, Markus Arndt, Anton Zellinger "Quantum interference experiments with large molecules" *Institut fur Experimentalphysik, Universitat Wien, Austria , Am J. Phys 71 (4),*April 2003.

[13] D. W. Keith, M. L. Schattenburg, Henry I. Smith, D. E. Pritchard "Diffraction of Atoms by a Transmission Grating" *Massachusetts Institute of Technology, Cambridge Massachusetts,* July 1988.